Two-Terminal Traveling-Wave-Based Non-Homogeneous Transmission-Line Protection

J. R. Lima Júnior, F. B. Costa, F. V. Lopes

***Abstract*—This paper presents a two-terminal traveling-wave-based protection algorithm applied to non-homogeneous transmission lines comprising any number of sections with different topologies and considering the effect of the sampling rate. Existing two-terminal traveling wave protection functions cannot protect the line under close-in faults and present limitations in non-homogeneous transmission lines. However, the effects of the sampling rate, considered in the proposed method, result in well-defined protection and unprotected zones, essential for protection security and coordination to deal with the issue of close-in faults in non-homogeneous transmission lines. Furthermore, the algorithm can accurately detect the faulted section, allowing its use in advanced protection functions such as adaptive automatic auto-reclosing and high-speed protection schemes. A protection device was modeled considering a sampling frequency equal to 1 MHz, including functions to detect traveling waves via wavelet transform, and the proposed protection algorithm to discriminate line internal from external faults, and to select the faulted section. The algorithm was evaluated using a large number of ATP fault simulations. The results show that the algorithm is robust and reliable for protection devices installed in non-homogeneous lines.**

***Keywords*—Hybrid Lines, Protection, Transmission Lines, Traveling Waves.**

I. Introduction

NON-homogeneous transmission lines (NHL) comprising sections with different topologies and electrical parameters are increasingly present to meet the most diverse demands for electricity. In power generation, for instance, the demand for cleaner energy has driven the construction of offshore power plants, which are often connected to the grid through lines formed by submarine cables and overhead sections. Similarly, in highly populated urban areas, where the population safety and the environmental/aesthetic constraints are an issue, lines with one or more underground and overhead sections have been used [1], [2]. As a result, the complexity of electrical transmission systems has increased significantly, especially for protection and fault location devices.

Several papers have reported solutions for application in NHL protection and fault location [3]–[8]. The most commonly used conventional protection for NHL uses distance and differential protection schemes. However, conventional phasor-based distance protections experience difficulties in dealing with NHL, mainly due to the grounding method and the characteristics of underground cable sections [9]. In addition, the calculation of the apparent impedance seen by the protection relay, especially in single-phase faults, becomes much more complex in NHL, requiring greater care in the relay settings [9]. Thus, in some cases, the traditional solution is not applicable or becomes too expensive. In order to overcome some drawbacks of the conventional approaches, [8] proposes a fault location and section identification algorithm for three-terminal hybrid lines that does not require information about the parameters of each section. The electrical parameters are estimated in a closed-loop calculation by comparing the pre-fault series impedance parameters. However, this paper does not address hybrid or non-homogeneous line protection.

In turn, techniques based on traveling waves or on time domain studies promise to be faster than conventional ones [10] and less affected by differences in the electrical parameters of different sections of the NHL. Several works have focused on the problem of fault location using such techniques. [7], [11], [12] proposes a fault location algorithm that uses an equivalent homogeneous line for fault location, in which the propagation time is equal to the sum of the individual propagation times of each section, applying the classical two-terminal equation considering an equivalent propagation velocity. [7] presents a generalized equation for fault location in NHL that can be applied to a line comprising any number of sections. It uses the classical two-terminals fault location equation, considering a homogeneous line with the parameters of a pre-identified fault section and adding a correction factor to eliminate the errors caused by line non-homogeneity. This paper also makes a comprehensive discussion of the uncertainties in the electrical parameters of transmission lines. It proposes the adoption of a user-defined minimum and maximum uncertainty limit setting in order to avoid misinterpretation of the fault location. However, the effects of the sampling rate are not analyzed, so that, depending on used rate, relevant inaccuracies in the fault location estimation can take place.

[13] presents an algorithm for homogeneous two-terminal transmission line protection based on traveling waves considering the effect of sampling rate and traveling-wave propagation velocity. It also comprehensively analyzes the errors associated with the time instants of the arrival of traveling waves. Considering the distance that a traveling wave travels in a sample time given a sampling rate, it is shown that the line can be subdivided into small sections proportional to the sampling frequency. With this approach, the authors demonstrate that there are regions very close to the line terminals where faults can be incorrectly detected if the sampling rate effects are not considered, leading to uncertainty. Also, protected and unprotected zones over the

Paper submitted to the International Conference on Power Systems Transients (IPST2023) in Thessaloniki, Greece, June 12-15, 2023.

line are demonstrated, adopting the speed of light as a conservative reference for the identification of faults inside the line. However, the case of non-homogeneous lines was not addressed. Besides, it is considered that the signals are perfectly synchronized and that there are no errors associated with detection algorithms, i.e., it is assumed that the incident waves are detected in the first sample right after the incident waves.

Practical applications for NHL or hybrid lines have been reported in [3], [14] using commercial protective relays with the TW-based differential function (TW87). The detection of the traveling waves is performed using the differentiator–smoother filter (DS filter) [15]. Although the results showed reliable and fast operation, the effect of the sampling rate was not addressed. Furthermore, the algorithm is recommended for hybrid lines with cable sections no longer than 2 km [16]. [17] presents an analysis of TW87 functions and highlights the reason for such a restriction when the TW87 is applied to hybrid lines. Hence, from the best knowledge of the authors, there are no papers that consider the effect of the sampling rates on protection schemes for NHLs.

This paper proposes a two-terminal traveling-wave-based protection applied to non-homogeneous transmission lines. By considering the effects of the sampling rate of the digital signals, the contributions of the proposed protection function are: 1) identification of protection zones and accurate protection for faults inside the protected zones; 2) identification of zones where close-in faults are not detected, allowing possible coordination with other protection systems for these cases; 3) protection of non-homogeneous transmission lines regardless of the number of line sections or its length; 4) identification of the faulted section, which is useful for advanced protection logics, such as selective automatic reclosing or high-speed protection schemes. The algorithm also accommodates synchronization and errors in the detection of the wavefront arrival times, leading to a reliable and fast protection operation.

II. Traveling Waves on NHL

Fig. 1 illustrates an NHL of length D between local (L) and remote (R) busbars comprising of m sections of length D_i ($i = 1 : m$), each one with different topologies and electrical parameters.

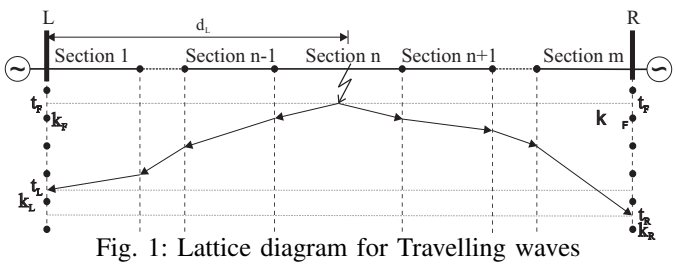

Fig. 1: Lattice diagram for Travelling waves

Given a fault in section n ($1 \leq n \leq m$), current and voltage waves travel from the fault point with limited propagation speed $v_n = 1/\sqrt{L_n C_n}$ ($v_n < c$), where L_n and C_n are, respectively, the series inductance in H/km and shunt capacitance in F/km of section n and c is the speed of light in vacuum. At the transition point between sections, the traveling waves undergo reflections and refractions according to the characteristic impedance of the line section and the electrical system ahead. Waves refracted to the forward section travel at a different speed due to different electrical parameters.

The total NHL propagation time τ_{NHL} is given by

$$\tau_{NHL} = \tau_1 + \tau_2 + ... + \tau_n + ... + \tau_m, \tag{1}$$

where $\tau_i = D_i/v_i$ are the propagation times of the traveling waves in each section $i = 1 : m$.

Consider a disturbance in section n at time t_F at a distance d_L from terminal L and d_R from terminal R. Voltage and current waves are generated and propagate toward both terminals of the line. The propagation time of the traveling waves from the fault point in section n to the L and R terminals, respectively, can be given by

$$\tau_L = \frac{D_1}{v_1} + \frac{D_2}{v_2} + ... + \frac{kD_n}{v_n}, \tag{2}$$

$$\tau_R = \frac{(1-k)D_n}{v_n} + \frac{D_{n+1}}{v_{n+1}} + ... + \frac{D_m}{v_m}, \tag{3}$$

where $k = 0..1$ is the percentage of the location of the fault in section n with reference to terminal L.

The protection devices installed at terminals L and R of the line detects the arrival of traveling waves at times t_L and t_R, respectively, which can be calculated by

$$t_L = t_F + \tau_L, \tag{4}$$

$$t_R = t_F + \tau_R. \tag{5}$$

Therefore, considering both terminals synchronized, for internal NHL faults, the following condition must be satisfied

$$|t_L - t_R| < \lfloor \tau_{NHL} \rfloor \tag{6}$$

and for external faults

$$|t_L - t_R| = \lfloor \tau_{NHL} \rfloor \tag{7}$$

Advanced protection functions require a correct identification of the section under fault. From (2) and (3), the difference between the measured times at each terminal $\Delta t = t_L - t_R$ is then

$$\Delta t = \frac{D_1}{v_1} + \frac{D_2}{v_2} + ... + \frac{kD_n}{v_n} - \frac{(1-k)D_n}{v_n} - \frac{D_{n+1}}{v_{n+1}} - ... - \frac{D_m}{v_m}, \tag{8}$$

That is, the time difference Δt can be calculated by combining the propagation times of the traveling waves in each section τ_i. Combining (1) and (8) yields

$$\Delta t = 2\frac{D_1}{v_1} + 2\frac{D_2}{v_2} + ... + 2\frac{kD_n}{v_n} - \tau_{NHL}. \tag{9}$$

Then, the limits of the section n can be found by the time difference Δt as follows:

$$k = 0 \rightarrow \Delta t = 2\sum_{i=1}^{n-1} \frac{D_i}{v_i} - \tau_{NHL}, \tag{10}$$

$$k = 1 \rightarrow \Delta t = 2\sum_{i=1}^{n} \frac{D_i}{v_i} - \tau_{NHL}. \tag{11}$$

Generalizing, the section under fault can be determined by

$$2\sum_{i=1}^{n-1}\frac{D_i}{v_i}-\tau_{NHL}\leq\Delta t\leq 2\sum_{i=1}^{n}\frac{D_i}{v_i}-\tau_{NHL} \tag{12}$$

Although fault location is not in the scope of this paper, the proposed method identifies the faulted section as an additional result, necessary in cases of permanent faults.

III. Sampling Rate Effects

Transmission line protection devices use discrete time variables instead of continuous time variables. Therefore, the sampling rate influences the accuracy and safety of the operation of protection devices and must be taken into account. The lower the sampling rate, the greater the errors in TW.

Considering Fig. 1, a fault occurs at an unknown time t_F. In the discrete domain, for a sampling rate f_s, the fault inception time becomes k_F/f_s ($k_F \in N$) instead t_F, resulting:

$$\frac{k_F}{f_s}=\frac{\lfloor t_F f_s\rfloor}{f_s}+\frac{1}{f_s}\rightarrow t_F<\frac{k_F}{f_s}\leq t_F+\frac{1}{f_s}, \tag{13}$$

where k_F is the first sample right after the fault inception time and $\lfloor *\rfloor$ is the largest integer not greater than $*$ (floor function).

The traveling waves from the fault point strike terminal L at time t_L and terminal R at time t_R. In the discrete time domain, t_L becomes k_L/f_s ($k_L \in N$), and t_R becomes k_R/f_s ($k_R \in N$). They are associated with the first sample affected by traveling waves in terminals L and R, respectively, as follows:

$$\frac{k_L}{f_s}=\frac{\lfloor t_L f_s\rfloor}{f_s}+\frac{1}{f_s}\rightarrow t_L<\frac{k_L}{f_s}\leq t_L+\frac{1}{f_s}, \tag{14}$$

$$\frac{k_R}{f_s}=\frac{\lfloor t_R f_s\rfloor}{f_s}+\frac{1}{f_s}\rightarrow t_R<\frac{k_R}{f_s}\leq t_R+\frac{1}{f_s}. \tag{15}$$

Therefore, there is an error between the actual times and those measured by the protection devices for a given sampling rate. The error associated with fault inception time due to the sampling process is given by:

$$\xi_{t_F}=\frac{k_F}{f_s}-t_F, \tag{16}$$

where $0\leq\xi_{t_F}<1/f_s$. At the same way, the errors associated to incident traveling waves at terminals L and R are

$$\xi_{t_{F_L}}=\frac{k_L}{f_s}-t_L, \tag{17}$$

$$\xi_{t_{F_R}}=\frac{k_R}{f_s}-t_R, \tag{18}$$

where $0\leq\xi_{t_{F_L}}<1/f_s$ and $0\leq\xi_{t_{F_R}}<1/f_s$.

By analyzing (17) and (18), the errors $\xi_{t_{F_L}}$ and $\xi_{t_{F_R}}$ are at most one sampling time, considering that the fault is detected in the sample right after the arrival of the incident wave. In order to take into account the possibility of protection do not identify that way, it is proposed the user-defined factor α, which can be set to a number of samples, depending on the security margin needed. If the protection decision is critical, a higher α setting probably should be adjusted. If it is considered that the incident wavefront will be detected only a few samples after, it has to be adjusted to a proper α. If other errors must be considered, like delayed detection due to dumped transients or even communication synchronization errors, the setting α could be used to accommodate such errors. Therefore $0\leq\xi_{t_{F_L}}<\alpha/f_s$ and $0\leq\xi_{t_{F_R}}<\alpha/f_s$.

In order to minimize the errors related above, high sampling rates have been used in modern protection devices [16]. However, those errors must be included in protection analysis as proposed in this paper since they can lead to a malfunction of protection algorithms. On the other hand, practical and economical devices operating with low sampling rates in the range of a few kilohertz are the most impacted. In that case, its consideration becomes even more critical.

A. Influence of Sampling Rate on Protection

In the discrete time domain, (6) must be corrected in order to take in account the sampling process errors indicated in (17) and (18). Thus, the time difference Δt becomes

$$\Delta t=t_L-t_R=(t_L-t_F)-(t_R-t_F), \tag{19}$$

$$\Delta t=\frac{1}{f_s}\left(k_L-k_R\right)+\left(\xi_R-\xi_L\right), \tag{20}$$

$$\Delta t=\frac{\Delta k}{f_s}+\Delta\xi, \tag{21}$$

where $\Delta\xi=\xi_R-\xi_L$ is the global error and $\Delta k=k_L-k_R$ is the difference between the detection samples of the traveling waves at terminals L and R. The global error $\Delta\xi$ can be estimated as detailed in Table I.

TABLE I: Errors Estimation

ξ_L	ξ_R	$\Delta\xi$
0	0	0
α/f_s	0	-α/f_s
0	α/f_s	+α/f_s
α/f_s	α/f_s	0

Thus, $-\alpha/f_s\leq\Delta\xi\leq\alpha/f_s$ Therefore, considering the discrete-time domain in (6), an internal fault on the NHL is detected if:

$$\left|(k_L-k_R)+f_s\Delta\xi\right|<\left\lfloor f_s\tau_{NHL}\right\rfloor. \tag{22}$$

B. Fault Section Pre-Identification Considering the Sampling Rate Effects

Considering the errors due to the sampling rate given in (17) and (18), the fault section pre-identification given in (12) can be rewritten in the discrete domain as follows:

$$2\sum_{i=1}^{n-1}f_s\frac{D_i}{v_i}-\tau_{NHL}f_s\leq\Delta k-\Delta\xi f_s\leq 2\sum_{i=1}^{n}f_s\frac{D_i}{v_i}-\tau_{NHL}f_s, \tag{23}$$

which shows the limits of section n and should be used to pre-indicate the fault section.

C. Protection Aplication

From (8), Δk can be rewritten as

$$\Delta k = \sum_{i=1}^{n-1} f_s \frac{D_i}{v_i} \pm f_s \frac{D_n}{v_n} - \sum_{i=n+1}^{m} f_s \frac{D_i}{v_i}, \tag{24}$$

where the $\pm$ sign in the D_n/v_n term is positive when the fault is at the end of section and negative when the fault is at the beginning of section, with reference to the terminal L. Rearranging and simplifying (24), gives

$$|\Delta k + \gamma| = \left\lfloor f_s \frac{D_n}{v_n} \right\rfloor, \tag{25}$$

where γ is a correction variable due to non-homogeneity of line parameters, given by

$$\gamma = \sum_{i=n+1}^{m} f_s \frac{D_i}{v_i} - \sum_{i=1}^{n-1} f_s \frac{D_i}{v_i}. \tag{26}$$

In practical terms, when the γ variable is added to the Δk, the protective devices are virtualy relocated from the line terminals to the ends of the previously indicated fault section. Therefore, the proposed protection algorithm can be fully applied to non-homogeneous lines. Once the discrete wavefront arrival times are detected, the external fault is detected if

$$|(k_L - k_R) + \gamma + f_s \Delta\xi| = \left\lfloor f_s \frac{D_n}{v_n} \right\rfloor, \tag{27}$$

Whereas, internal faults can be detected if

$$|(k_L - k_R) + \gamma + f_s \Delta\xi| < \left\lfloor f_s \frac{D_n}{v_n} \right\rfloor, \tag{28}$$

where $\Delta\xi$ depends on t_F which is an unknown variable.

D. The Section Subdivision due to Sampling Rate

In the time associated with one sample for a given sampling frequency f_s, the traveling waves travel a distance in section n given by

$$\Delta d_n = v_n / f_s, \tag{29}$$

where $\Delta d_n \leq D_n$ and $f_s \geq v_n / D_n$. Thus, the length of the section can be subdivided into K small portions of size Δd_n, where K is given by

$$K = \left\lfloor \frac{D_n}{\Delta d_n} \right\rfloor = \left\lfloor f_s \frac{D_n}{v_n} \right\rfloor. \tag{30}$$

Since the length of each section is not necessarily a multiple of Δd_n, there must be a complement Δd_{n2} at each end of the section given by

$$\Delta d_{n2} = \frac{D_n}{2} - K \Delta d_{n1} = \frac{L_n}{2} - \left\lfloor f_s \frac{D_n}{v_n} \right\rfloor \frac{v_n}{2 f_s}, \tag{31}$$

where $\Delta d_{n1} = \Delta d_n / 2$ and $0 \leq \Delta d_{n2} < v_n / 2 f_s$.

The section is therefore subdivided into small portions proportional to the sampling rate and its total length is

$$D_n = \Delta d_{n2} + 2K \Delta d_{n1} + \Delta d_{n2}. \tag{32}$$

Fig. 2 illustrates the section splitting due to the sampling rate effect.

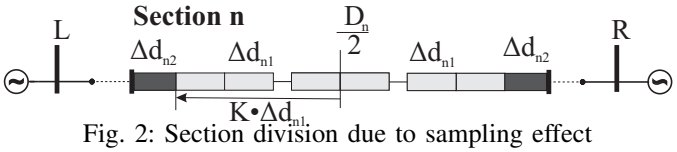

Fig. 2: Section division due to sampling effect

Internal faults to the section n are identified when

$$\Delta d_{n2} + |\Delta\xi|\, v_n/2 < d_L < D_n - \Delta d_{n2} - |\Delta\xi|\, v_n/2. \tag{33}$$

Therefore, analyzing (33), there is an Unprotected Zone Δd_{n2} at both ends of each section in which faults are not detected due to the error associated with the sampling effect. Similarly, faults located $\alpha \Delta d_{n1}$ after the unprotected zones can be declared as internal or external to the section, depending on the instant of the fault t_f. This is the Uncertainty Zone. In turn, faults located between $\Delta d_{n2} + \alpha \Delta d_{n1}$ and $D_n - \Delta d_{n2} - \alpha \Delta d_{n1}$ are always identified as internal to the section, and are then considered as in the Protected Zone.

IV. Performance Evalution

To evaluate the proposed algorithm performance, a 380 kV/50 Hz electrical system shown in Fig. 3 was modeled in ATP. The NHL is composed by two overhead sections, one underground cable section, and one submarine cable section.

A. Modeled Electrical System

The overhead line sections were considered according to [18]. It is a simple circuit with horizontally arranged conductors and a tower span of 400 m. Each phase consists of a triplet bundle of ACSR conductors (Cross-section = 31.5 mm) in symmetrical triangular formation with 40 cm conductor spacing. The height of the tower is 36 m and the horizontal spacing between phases is 7.4 m. Two galvanized steel shield wires (Cross-sectiom = 11.5 mm) were used. The soil resistivity was considered to be 500 Ω.m.

The model used for the simulation of the submarine cables was proposed in [19]. It is a Cu 1000 mm^2 Low Pressure Fluid Filled cable (LPFF) (Pb sheath + Al armor). The wires are at a depth of 300 m and are horizontally spaced 20 m apart. According to [20], the electrical resistivity of seawater is between 0.01 to 0.000025 times ground resistivity. Thus, the electrical resistivity of the seawater considered was $\rho_m = 0.5$ Ω·m, as used in [7].

The underground line section was modeled according [18] and is a single circuit buried at 1.5 m composed by three single-core 380 kV XLPE-insulated cables (2500 mm^2 Cu) in horizontal flat configuration with 0.35 m spacing. The ground resistivity is 50 Ωm

All line sections were modeled using the Jmarti model with distributed frequency-dependent parameters, with initial frequency of 0.5 Hz and the maximum frequency 1 MHz. Six decades and 10 points per decade were used for the numerical solution. Although the model is frequency-dependent, the transformation matrix is real and tuned to the steady state frequency of 50 Hz. The propagation velocity v_p of each section was obtained from the power-up tests, according to [16] and are shown in Table II.

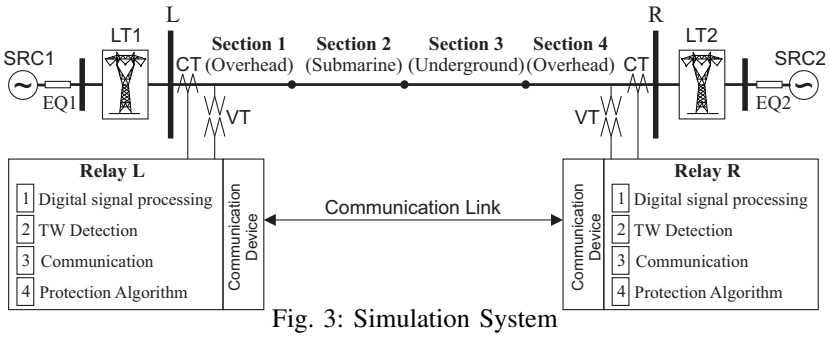

Fig. 3: Simulation System

TABLE II: NHL Section Parameters

Section	Topology	Length (km)	v_p (km/s)
1	Overhead	12	$2.95570e+05$
2	Submarine	3.7	$1.85930e+05$
3	Underground	5	$1.93050e+05$
4	Overhead	12	$2.95570e+05$

The NHL was covered with a light load of 10 degrees from the L-busbar to the R-busbar, maintaining the voltages in the buses at 1 pu. The CT and CCVT transducers were modeled to make the simulations more realistic. The CTs was set at 2000-5 A and the CCVTs at 380 kV/115 V. Both currents and voltages can be used by the traveling wave arrival time detection method, which is out of the scope of this paper. The used detection method needs only currents.

B. Fault Simulations

The time step used in the fault simulations was 0.1 μs, equivalent to a sampling rate of 10 MHz. This time step is ten times smaller than the sampling time ($1/f_s$=1 μs) used in the protection algorithm. In this way, the fault inception time in the simulations is in the continuous-time domain from the point of view of the proposed protection algorithm, which is essential to consider the effects of the sampling rate.

The proposed method performance evaluation considered a total of 1020 faults along the NHL. 810 faults were single-line-to-ground faults (AG faults), given their greater incidence in transmission lines [21]. Similarly, in underground cables, most faults are single-line-to-ground ones [9]. Additionally, 210 cases of phase-to-phase faults (BC faults) were also considered. The protection algorithm works with any type of fault since only the time associated with the first incident wave at each terminal is required.

The fault type, fault-inception angle, and fault resistance affect the performance of the first wavefront arrival time detection method, which is out of the scope of this paper. Therefore, these parameters were not evaluated in this paper, and the simulations considered fault inception angle of 90° and low-resistance faults. Since the ATP does not allow null resistance, the fault resistance was set to 0.1 Ω.

To include the effects of the sampling rate, it is necessary to simulate faults with different fault inception times between two consecutive sampling times in a continuous-time domain. Considering the used simulation time step of 0.1 μs and the relay sampling time of 1 μs, it is possible to simulate ten faults with different fault inception times between two relay sampling times. To do it, the fault inception angle was varied slightly around 90° just enough to obtain a time difference of one sample between each fault simulation, keeping the same fault location. That is, for 50 Hz systems and a time step of 0.1 μs, the angle difference $\Delta\theta = \omega\Delta t = 50 \times 360 \times 0.1 \times 10^{-}6 = 0.0018°$. In this way, for the same fault location, 10 simulations are obtained with fault instants one time step away from each other.

The location of the faults was chosen to obtain at least one fault in each of the predicted zones (unprotected zone, uncertainty zone and protected zone) and at each transition point. Table III shows the fault location at each section.

C. Algorithm Settings

In the digital signal processing, a random white Gaussian noise of SNR 60 db has been added to the voltage and current signals. For the discretization, a 2-order Butterwolf Anti-aliasing filter with a cutoff frequency set at 80 % of the Nyquist frequency, thus at 400 kHz, was used.

The detection of the wavefronts of traveling waves is out of scope of this paper. To identify the traveling waves, the stationary boundary wavelet transform (SBWT) was choosed, according to [22]. The algorithm analyzes the energy of the 1-scale wavelet coefficients. The traveling wavelet detection threshold was set to $\lambda = \mu + 5\sigma$, where μ is the mean and σ is the standard deviations calculated on a fundamental cycle

TABLE III: Simulation fault location in km

Predicted Zone	Section 1 [km]	Section 2 [km]	Section 3 [km]	Section 4 [km]
Unprotected	0.0000	12.0000	15.7000	20.7000
	0.0500	12.0500	15.7500	20.7500
	0.0885	12.0837	15.7869	20.7886
Uncertainty	0.1200	12.1100	15.8100	20.8200
	0.1600	12.1400	15.8400	20.8600
	0.2000	12.1700	15.8700	20.9000
	0.2363	12.1766	15.8834	20.9364
Protected	0.3000	12.2000	16.0000	21.0000
	2.2000	12.8000	16.8000	22.9000
	4.1000	13.4000	17.6000	24.8000
	6.0000	13.8500	18.2000	26.7000
	7.9000	14.4000	18.9000	28.6000
	9.8000	14.9000	19.6000	30.5000
	11.7000	15.5000	20.4000	32.4000
Uncertainty	11.7637	15.5234	20.5166	32.4636
	11.7840	15.5270	20.5210	32.4840
	11.8040	15.5300	20.5240	32.5040
	11.8230	15.5330	20.5270	32.5230
Unprotected	11.9115	15.6163	20.6131	32.6114
	11.9600	15.6600	20.6600	32.6600
	12.0000	15.7000	20.7000	32.7000

at 50 Hz sliding window, as proposed in [23]. In this way, the detection threshold is immune to signal noise.

The protection algorithm requires the correct detection of the time instants associated with the incident waves at each end. Therefore, any detection technique that guarantees this premise can be used. The algorithm starts after the detection of traveling waves. When the first incident wave is detected at one of the terminals, the sample associated with the detection instant is transmitted to the remote terminal and the algorithm waits for the arrival of the sample detected by the remote terminal. The communication between both terminals should preferably be via a dedicated path and with deterministic communication time.

With the sampling index from the remote terminal, the algorithm calculates the difference $\Delta k = k_L - k_R$ and computes the associated error including the user-defined α variable. Then it is compared with the number of samples expected for internal faults, according to (22). If the fault is detected as internal to the NHL, the circuit breakers are tripped.

In parallel, the fault section detection algorithm starts. The pre-location of the fault section is done according to (23). After that, according to (25), adding the γ factor to the Δk it is possible to isolate the pre-identified section for validation by the protection algorithm. If $|\Delta k + \gamma| < \lfloor f_s L_n / v_n \rfloor - \alpha$, then the fault is declared internal to that section, allowing the use of advanced protection logics. For example, auto-reclosing can be blocked or tripping can be delayed if desired. The α factor can be set to more than 1 sample if desired. If the detection method delays both terminals by one sample, the difference in Δk cancels out this effect. However, if on one terminal the detection method is one sample ahead and the remote terminal is one sample behind, the difference Δk will have an error of 2 samples. Therefore, the α factor can be increased to accommodate this type of error.

D. Case Study - Internal Fault on Section 3

In order to better understand how the algorithm works, a case study involving a single-phase A-G fault near the middle of NHL, located at 16.8 km from terminal L, within section 3 is presented. The fault was simulated with a 90° incidence angle and occurred at sample 602,852 for a time step of 0.1 μs. In the time scale of the protection relays with a sampling rate of 1 MHz, the instant of the fault is associated with sample 60,286, which corresponds to sample 602,860 at the original time. Thus there is an error of 8 samples associated with the fault instant. Fig. (4) shows the currents at each terminal and the energy of the wavelet coefficients.

The protection device at the L terminal detects the first traveling wave at index sample 60,352. Similarly, the protection device installed at the remote R terminal detects the first incident wave on the 60,347 index sample. Both devices are synchronized. Therefore, as soon as the protective device receives the sample information from the remote terminal R it calculates the sample difference $\Delta k = k_L - k_R = 60,352 - 60,347 = 5$ samples.

Accounting for the error associated with the sampling effect of $\alpha = 1$, the algorithm compares Δk to the NHL propagation

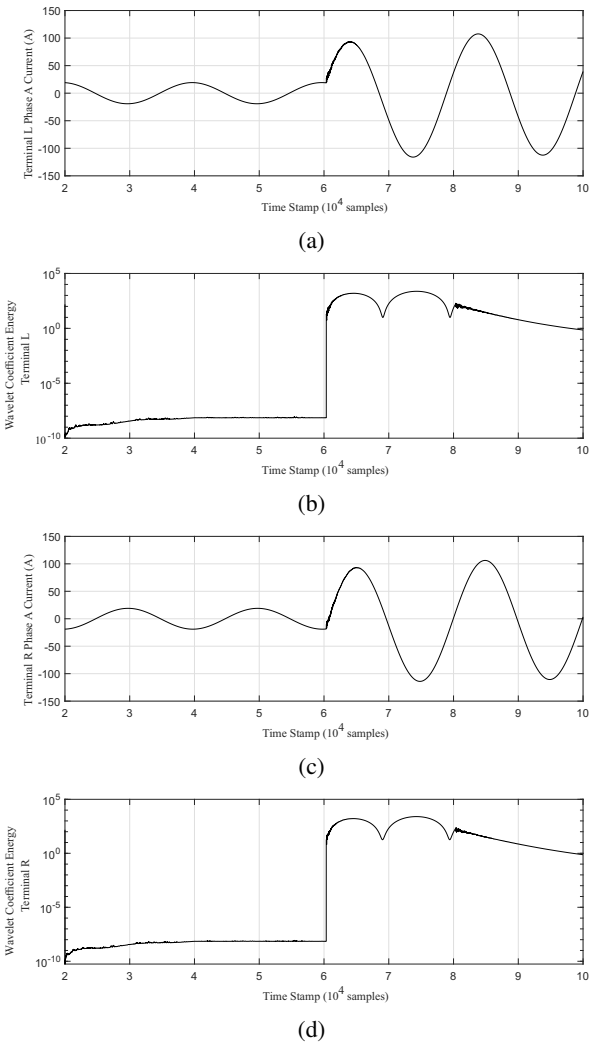

Fig. 4: Simulation of Internal Fault in Section 3: (4a) Phase A fault current at terminal L; (4b) Wavelet Coefficient Energy - Terminal L; (4c) Phase A fault current at terminal R; (4d) Wavelet Coefficient Energy - Terminal R.

time. If the condition in equation (22) is satisfied, then the protection algorithm declares the fault as internal and promotes the trip on the local circuit and remote breakers. The exact process takes place at the remote terminal.

The fault section pre-identification algorithm parallel computes the Δk variable and compares it with the limits of each section. In this case, $-4 < \Delta k < 43$ samples, configuring a fault in section 3.

In this way, the protection algorithm validates the fault section by computing the γ factor due to the non-homogeneity of the line. For section 3, $\gamma = -20$. According to equation (28), $|\Delta k + \gamma| < \lfloor f_s L_n / v_n \rfloor - \alpha \Rightarrow |5 - 20| < \left\lfloor 10^6 \times 5 / 1.93050 \times 10^5 \right\rfloor - 1 \Rightarrow 15 < 24$. Therefore the fault is confirmed in section 3. This information can then be used to block or enable automatic reclosing, for example.

With respect to processing time, the traveling wave detection algorithm processed the information in less than 0.3 ms. In turn, the algorithm for protection and identification of the fault

section processed the information in 43 μs.

The processing time of the communication devices was considered as 1 ms and the propagation time of the communication channels for the 32.7 km NHL was considered as 160 μs, taking as a reference the speed of light in fiber optics approximately 200,000 km/s.

Considering the time of the communication devices of 160 μs + 1 ms per SDH (Synchronous Optical Networking devices), the total time of the protection system was 2.503 ms.

E. Sensitivity Analysis Results

As aforementioned, 1020 faults were simulated along the NHL: 810 simulations were AG faults (190 faults on each of the four sections and 10 faults on each of the five transition points), and 210 simulations were BC faults on section 1 (190 on its section and 10 faults at its ends). Tables IV to VIII summarize the results for the protection function (Protection trip for internal faults) and the identification of the faults in the line sections. For each fault location, ten simulations were performed at different time instants.

Table IV shows the results in section 1, where all the simulated cases (30 cases) in the unprotected zone were successfully detected as external faults by the proposed protection function.

For faults in the uncertainty zones in Table IV, faults closer to the ends of the section are more likely to be detected as external. As the location of the fault moves towards the protected zone, the faults tend to be detected as internal to the section. This is due to the effect of the sampling rate and the inception time of the fault. For instance, for the 10 cases simulated at 160 m from terminal L, therefore, in the uncertainty zone of section 1, 8 cases were detected as external to the section, and 2 cases were detected as internal to the section. Therefore, the protection issued the trip two times in these cases. On the other hand, for the 10 cases located at 236.3 m from terminal L, at the edge of the uncertainty zone of section 1, only 1 case was detected as external, whereas 9 cases were detected as internal. Thus, the protection issued a trip nine times in these cases. This behavior explains the existence of the uncertainty zone due to the effects of the sampling rate.

In turn, all 140 simulations performed in the protected zone in Table IV were correctly detected as internal to section 1, as expected, and the protection issued a trip.

The same analysis done for the fault cases in section 1 can be extended to the fault cases in the other sections. The results for sections 2 and 3 are presented in tables V, VI, respectively. Since these sections are internal sections, they have only a protected zone, and all the faults were detected as internal faults by the proposed protection function. Section 4 (Table VII) is an external section, presenting unprotected, uncertain, and protected zones such as in section 1, and the protection and the fault section identification performed as expected.

These results are important because they clearly show the effect of the sampling rate and enable the engineer to reliably define the range of traveling wave protection zones, similar to what is done in conventional distance protection, for example. Additionally, BC faults were analyzed in section 1, showing that the algorithm is independent of the fault type. Table VIII shows similar results to those found for AG faults.

TABLE IV: Results for Faults on Section 1 - AG Faults

Predicted Zone	Fault Point	Protection Trip	Section 1		Number of Simulations
			Inside	Outside	
Unprotected	0.0000	0	0	10	10
	0.0500	0	0	10	10
	0.0885	0	0	10	10
Uncertainty	0.1200	0	0	10	10
	0.1600	2	2	8	10
	0.2000	5	5	5	10
	0.2363	9	9	1	10
Protected	0.3000	10	10	0	10
	2.2000	10	10	0	10
	4.1000	10	10	0	10
	6.0000	10	10	0	10
	7.9000	10	10	0	10
	9.8000	10	10	0	10
	11.7000	10	10	0	10
	11.7637	10	8	2	10
	11.7840	10	8	2	10
	11.8040	10	6	4	10
	11.8230	10	4	6	10
	11.9115	10	0	10	10
	11.9600	10	0	10	10
	12.0000	10	0	10	10

TABLE V: Results for Faults on Section 2 - AG Faults

Predicted Zone	Fault Point	Protection Trip	Section 2		Number of Simulations
			Inside	Outside	
Protected	12.0000	10	0	10	10
	12.0500	10	0	10	10
	12.0837	10	0	10	10
	12.1100	10	0	10	10
	12.1400	10	0	10	10
	12.1700	10	3	7	10
	12.1766	10	4	6	10
	12.2000	10	6	4	10
	12.8000	10	10	0	10
	13.4000	10	10	0	10
	13.8500	10	10	0	10
	14.4000	10	10	0	10
	14.9000	10	10	0	10
	15.5000	10	10	0	10
	15.5234	10	8	2	10
	15.5270	10	8	2	10
	15.5300	10	7	3	10
	15.5330	10	6	4	10
	15.6163	10	0	10	10
	15.6600	10	0	10	10
	15.7000	10	0	10	10

TABLE VI: Results for Faults on Section 3 - AG Faults

Predicted Zone	Fault Point	Protection Trip	Section 3		Number of Simulations
			Inside	Outside	
Protected	15.7000	10	0	10	10
	15.7500	10	0	10	10
	15.7869	10	0	10	10
	15.8100	10	0	10	10
	15.8400	10	0	10	10
	15.8700	10	3	7	10
	15.8834	10	4	6	10
	16.0000	10	6	4	10
	16.8000	10	10	0	10
	17.6000	10	10	0	10
	18.2000	10	10	0	10
	18.9000	10	10	0	10
	19.6000	10	10	0	10
	20.4000	10	10	0	10
	20.5166	10	8	2	10
	20.5210	10	8	2	10
	20.5240	10	7	3	10
	20.5270	10	6	4	10
	20.6131	10	0	10	10
	20.6600	10	0	10	10
	20.7000	10	0	10	10

TABLE VII: Results for Faults on Section 4 - AG Faults

Predicted Zone	Fault Point	Protection Trip	Section 4		Number of Simulations
			Inside	Outside	
Protected	20.7000	10	0	10	10
	20.7500	10	0	10	10
	20.7886	10	0	10	10
	20.8200	10	0	10	10
	20.8600	10	4	6	10
	20.9000	10	6	4	10
	20.9364	10	9	1	10
	21.0000	10	10	0	10
	22.9000	10	10	0	10
	24.8000	10	10	0	10
	26.7000	10	10	0	10
	28.6000	10	10	0	10
	30.5000	10	10	0	10
	32.4000	10	10	0	10
Uncertainty	32.4636	10	7	3	10
	32.4840	10	6	4	10
	32.5040	10	4	6	10
	32.5230	10	4	6	10
Unprotected	32.6114	10	0	10	10
	32.6600	10	0	10	10
	32.7000	10	0	10	10

TABLE VIII: Results for Faults on Section 1 - BC Faults

Predicted Zone	Fault Point	Protection Trip	Section 1		Number of Simulations
			Inside	Outside	
Unprotected	0.0000	10	0	10	10
	0.0500	10	0	10	10
	0.0885	10	0	10	10
Uncertainty	0.1200	10	0	10	10
	0.1600	10	2	8	10
	0.2000	10	5	5	10
	0.2363	10	9	1	10
Protected	0.3000	10	10	0	10
	2.2000	10	10	0	10
	4.1000	10	10	0	10
	6.0000	10	10	0	10
	7.9000	10	10	0	10
	9.8000	10	10	0	10
	11.7000	10	10	0	10
	11.7637	10	8	2	10
	11.7840	10	8	2	10
	11.8040	10	6	4	10
	11.8230	10	4	4	10
	11.9115	10	0	10	10
	11.9600	10	0	10	10
	12.0000	10	0	10	10

F. External Faults

Faults located at busbars L and R are physically external to the protected line, given the position of the CTs. Therefore, 20 simulations of faults external to the protected line were performed. The results for external faults are shown in Tables IV and VII for faults located at 0 km and 32.7 km, respectively. In both cases, the 20 simulated external fault cases were detected correctly by the algorithm as external and no trip was issued.

V. Conclusions

A two-terminal traveling-wave-based protection applied to non-homogeneous transmission lines irrespective of the number of line sections and taking into account the effect of sampling rate was presented. Consideration of the sampling rate allows the range of traveling wave protection to be defined more accurately and reliably, mainly when applied to non-homogeneous transmission lines, allowing its use in existing devices. The proposed method also identifies the fault section and accommodates synchronization and detection errors. A large number of fault-induced simulations were carried out in ATP and have been performed using a realistic model system. The results demonstrated that the proposed algorithm was fast, accurate, and reliable. Also, it was able to correctly identify the fault section, being useful in advanced protection schemes such as selective autoreclose. In future work, the performance of the developed algorithm can be compared to that of existing devices.

References

[1] H. Livani and C. Y. Evrenosoglu, "A machine learning and wavelet-based fault location method for hybrid transmission lines," *IEEE Trans. Power Del.*, vol. 5, no. 1, pp. 51–59, 2014.

[2] J. Han and P. A. Crossley, "Fault location on mixed overhead line and cable transmission networks," in *IEEE Grenoble Conf*, 2013, pp. 1–6.

[3] S. Sharma, A. Kathe, T. Joshi, and T. Kanagasabai, "Application of ultra-high-speed protection and traveling-wave fault locating on a hybrid line," in *46th Western Protective Relay Conference*, 2019.

[4] B. Patel and P. Bera, "Fast fault detection during power swing on a hybrid transmission line using wpt," *IET Generation, Transmission & Distribution*, vol. 13, no. 10, pp. 1811–1820, 2019.

[5] J. Han and P. A. Crossley, "Fault location on a mixed overhead and underground transmission feeder using a multiple-zone quadrilateral impedance relay and a double-ended travelling wave fault locator," in *IET Conference (DPSP)*, 2014, pp. 1–6.

[6] O. D. Naidu, A. K. Pradhan, and P. Krishnamurthy, "Traveling wave based adaptive auto-reclosing and fault location for three-terminal mixed lines," in *IEEE PES GTD Grand International Conf. and Exposition Asia (GTD Asia)*, 2019, pp. 466–471.

[7] E. J. S. Leite, F. V. Lopes, F. B. Costa, and W. L. A. Neves, "Closed-form solution for traveling wave-based fault location on non-homogeneous lines," *IEEE Trans. Power Del*, vol. 34, no. 3, pp. 1138–1150, 2019.

[8] K. Likhitha and O. D. Naidu, "Setting free fault location for three-terminal hybrid transmission lines connected with conventional and renewable resources," *IEEE*, vol. 11, pp. 23 839–23 856, 2023.

[9] D. A. Tziouvaras and J. Needs, "Protection of mixed overhead and underground cable lines," in *IET Conference (DPSP)*, 2014, pp. 1–6.

[10] E. O. Schweitzer, B. Kasztenny, A. Guzmán, V. Skendzic, and M. V. Mynam, "Speed of line protection - can we break free of phasor limitations?" in *68th Conf. for Prot. Relay Engineers*, 2015, pp. 448–461.

[11] H. G. S. Zhang and Y. Song, "A new fault-location algorithm for extrahigh-voltage mixed lines based on phase characteristics of the hyperbolic tangent function," *Trans. Power Del.*, vol. 31, no. 3, pp. 1203–1212, 2016.

[12] R. J. Hamidi and H. Livani, "Traveling-wave-based fault-location algorithm for hybrid multiterminal circuits," *IEEE Trans. Power Del*, vol. 32, no. 1, pp. 135–144, 2017.

[13] F. B. Costa, A. Monti, F. V. Lopes, K. M. Silva, P. Jamborsalamati, and A. Sadu, "Two-terminal traveling-wave-based transmission-line protection," *Trans. Power Del*, vol. 32, no. 3, pp. 1382–1393, 2017.

[14] E. O. Schweitzer, B. Kasztenny, and M. V. Mynam, "Performance of time-domain line protection elements on real-world faults," in *69th Conf. for Protective Relay Engineers (CPRE)*, 2016, pp. 1–17.

[15] E. O. Schweitzer, A. Guzmán, M. V. Mynam, V. Skendzic, B. Kasztenny, and S. Marx, "Locating faults by the traveling waves they launch," in *67th Conf. for Protective Relay Engineers*, 2014, pp. 95–110.

[16] Schweitzer, *SEL-T400L Ultra-High-Speed Line Relay*, Schweitzer.

[17] C. M. S. Ribeiro, F. V. Lopes, and J. P. G. Ribeiro, "Traveling wave-based differential protection applied to hybrid transmission lines: Performance and setting studies," in *2018 SBSE*, 2018, pp. 1–6.

[18] L. Colla, F. M. Gatta, A. Geri, and S. Lauria, "Lightning overvoltages in hv-ehv mixed overhead-cable lines," 2017.

[19] T. Ohno, "Dynamic study on the 400 kv 60 km kyndbyværket – asnæsværket line," Ph.D. dissertation, 2012.

[20] J. Vargas, A. Guzman, and J. Robles, "Underground/submarine cable protection using a negative-sequence directional comparison scheme," in *26th Western Protective Relay Conference*, 1999, pp. 2–68.

[21] B. J. Lewis and T. J. Domin, *Principles and Applications (version 4th ed)*, 01 2014, vol. 4.

[22] F. B. Costa, "Fault-induced transient detection based on real-time analysis of the wavelet coefficient energy," *IEEE Trans. Power Del*, vol. 29, no. 1, pp. 140–153, 2014.

[23] ——, "Boundary wavelet coefficients for real-time detection of transients induced by faults and power-quality disturbances," *IEEE Trans. Power Del*, vol. 29, no. 6, pp. 2674–2687, 2014.